New Model for the Analysis of Size-Scale Effects on the Ductility of Reinforced Concrete Elements in Bending

A. Carpinteri, F.ASCE[1]; M. Corrado[2]; M. Paggi[3]; and G. Mancini[4]

Abstract: The well-known *cohesive crack model* describes strain localization with a softening stress variation in concrete members subjected to tension. An analogous behavior is also observed in compression, when strain localization takes place in a damaged zone and the stress reaches the compression strength with surface energy dissipation. In the present paper, we propose the new concept of *overlapping crack model,* which is analogous to the cohesive one and permits us to simulate material interpenetration due to crushing. The two aforementioned elementary models are merged into a more complex algorithm able to describe both cracking and crushing growths during loading processes in reinforced concrete members. A numerical procedure based on elastic coefficients is developed, taking into account the proposed constitutive laws in tension and compression. With this algorithm, it is possible to effectively capture the flexural behavior of reinforced concrete beams by varying the reinforcement percentage and/or the beam depth.

DOI: 10.1061/(ASCE)0733-9399(2009)135:3(221)

CE Database subject headings: Reinforced concrete; Ductility; Size effect; Crushing; Nonlinear analysis; Finite element method; Bending.

Introduction

The development of considerable ductility in the ultimate limit state is a key parameter for the design of reinforced concrete (RC) beams in bending (Corley 1966; Macchi 1969; Eligehausen and Langer 1987; Hillerborg 1990; Bigaj and Walraven 1993). However, the assessment of the available ductility and the corresponding moment redistribution is complicated by the contemporaneous presence of different nonlinear contributions: crack opening in tension, concrete crushing in compression and steel yielding or slippage. Very often, the concrete contribution in tension is totally neglected or just considered with a linear–elastic stress–strain law until the ultimate tensile strength is reached. The nonlinear concrete behavior in compression is certainly not negligible. Several laws may be used to model the concrete behavior in compression: elastic–perfectly plastic, parabolic–perfectly plastic, Sargin's parabola, etc. As far as the steel behavior is concerned, the most used constitutive laws are the elastic–perfectly plastic or the elastic-hardening stress-strain relationships. The implementation of these constitutive laws in the finite-element method permits to describe the behavior of a RC member, although it is difficult to model the experimentally observed size-scale effects on the ductility of RC beams in bending. One of the main reasons for this is represented by the fact that the aforementioned constitutive laws consider only an energy dissipation over the volume in the nonlinear regime.

On the other hand, the application of fracture mechanics concepts has been proven to be very effective for the analysis of size-scale effects in concrete and reinforced concrete structures. Most of the applications concern the analysis of the ductile-to-brittle transition in unreinforced concrete beams in bending (Carpinteri 1985, 1989), the assessment of the shear resistance (Gustafsson and Hillerborg 1988; Jenq and Shah 1989; Bazant and Kim 1984; Carpinteri et al. 2007), and the evaluation of the minimum reinforcement (Bosco et al. 1990; Bosco and Carpinteri 1992; Carpinteri 1999) of RC beams. With regard to the behavior of concrete in compression, Hillerborg (1990) first introduced a model based on the concept of strain localization for the analysis of overreinforced beams in bending. According to his approach, when the ultimate compression strength is achieved, a strain localization takes place within a characteristic length proportional to the width of the compression zone. This model permits to address the issue of size effects, although the definition of the length over which the strain localization occurs is a free parameter and its value is not defined on the basis of theoretical arguments.

Further, many experimental tests put into evidence that a significant scale effect on the dissipated energy density takes place (see, e.g., Dahl and Brincker 1989; van Vliet and van Mier 1996; Carpinteri et al. 2005; Suzuki et al. 2006). The dissipated energy density can be assumed as a material constant only if it is defined as a crushing surface energy. Hence, we herein explore the possibility to model the process of concrete crushing using an approach similar to the cohesive model, which is adopted for the tensile behavior of concrete. In particular, we define a linear–elastic stress–strain law, before achieving the compression

[1]Professor of Structural Mechanics, Dept. of Structural Engineering and Geotechnics, Politecnico di Torino, Corso Duca degli Abruzzi 24, 10129, Torino, Italy. E-mail: alberto.carpinteri@polito.it

[2]Postdoctoral Fellow, Dept. of Structural Engineering and Geotechnics, Politecnico di Torino, Corso Duca degli Abruzzi 24, 10129, Torino, Italy.

[3]Assistant Professor of Structural Mechanics, Dept. of Structural Engineering and Geotechnics, Politecnico di Torino, Corso Duca degli Abruzzi 24, 10129, Torino, Italy.

[4]Professor of Structural Design, Dept. of Structural Engineering and Geotechnics, Politecnico di Torino, Corso Duca degli Abruzzi 24, 10129, Torino, Italy.

Note. Associate Editor: George Z. Voyiadjis. Discussion open until August 1, 2009. Separate discussions must be submitted for individual papers. The manuscript for this paper was submitted for review and possible publication on August 2, 2007; approved on October 15, 2008. This paper is part of the ***Journal of Engineering Mechanics***, Vol. 135, No. 3, March 1, 2009. ©ASCE, ISSN 0733-9399/2009/3-221–229/$25.00.

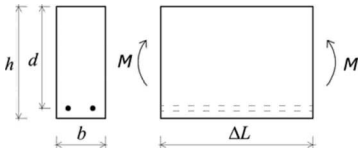

Fig. 1. Scheme of a reinforced concrete element

strength. Afterward, a descending stress–displacement law is introduced, for the analysis of the nonlinear behavior of concrete in compression.

Finally, special mention has to be given to the steel–concrete interaction. The most appropriate law for the reinforcing bar bridging a tensile crack propagating in concrete is a nonlinear relationship between force and crack opening. This relationship can be deduced from bond–slip laws and can be suitably included in the numerical algorithm as a modification of the constitutive behavior of the node of the finite-element mesh where the steel reinforcement is present. In this framework, multiple levels of reinforcement can be easily taken into account.

In the next sections we propose a new step-by-step numerical method able to describe the behavior of a reinforced concrete member during both fracturing and crushing. First, the *cohesive crack model* for concrete in tension and the *overlapping crack model* for concrete in compression are introduced, as well as the stress–displacement relationship for steel in tension. A numerical algorithm based on the finite-element method is presented for the analysis of all the intermediate situations ranging from pure concrete members to overreinforced beams. It is assumed that the fracturing and crushing processes are fully localized along the midspan cross section of the representative structural element in bending. This assumption, fully consistent with the crushing phenomenon, also implies that only one equivalent main tensile crack is considered. The results of the parametric investigations are reported in useful nondimensional diagrams showing the influence of the reinforcement percentage and of the structural size on the ductility of RC members in bending. Finally, a comparison between the numerical predictions and the results of the experimental tests carried out on RC beams in bending by Bosco and Debernardi (1992) is carried out in order to validate the proposed model. Future developments and perspectives conclude the paper.

Description of the Proposed Model

Let us consider the reinforced concrete beam segment shown in Fig. 1 and subjected to a bending moment M. This element, having a length equal to the beam depth, is representative of the zone where a plastic hinge formation takes place. The analysis of this structural element is consistent with the prescriptions reported in the Eurocode 2 (EN 1992) for the evaluation of the plastic rotation capacity of RC beams in bending. We also assume that the midspan cross section of this element could be fully representative of its mechanical behavior. The stress distribution is linear–elastic until the tensile stress at the soffit reaches the concrete tensile strength. When this threshold is reached, a cohesive crack propagates from the beam soffit toward its extrados. Correspondingly, the applied moment increases. Outside the crack, the material is assumed to behave elastically [Fig. 2(a)]. According to the well-known cohesive model, the stresses in the cohesive zone are assumed to be a function of the crack-opening displacement and

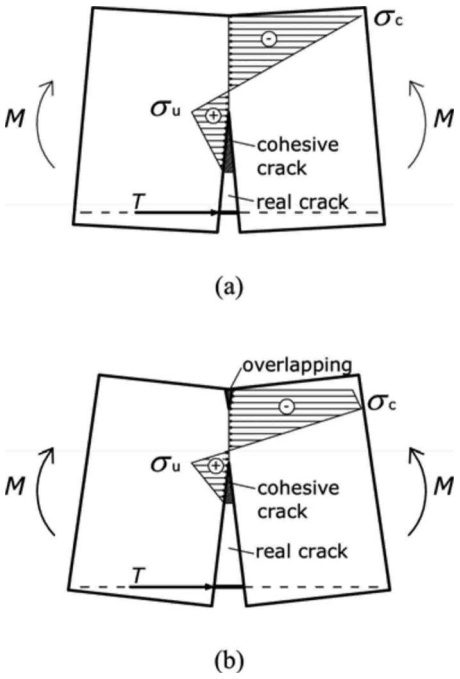

Fig. 2. Cohesive stress distribution in tension with: (a) linear–elastic distribution in compression; (b) nonlinear behavior in tension and compression

become equal to zero when the crack-opening displacement is larger than a critical value.

On the other hand, the damage phenomenon leading to concrete crushing begins when the maximum stress in compression reaches the concrete compression strength. Afterward, the development of microcracking up to full fragmentation takes place with a subsequent reduction of the stresses in the compression zone. Damage is then described as a fictitious interpenetration of the two half-beams, representing the localization of the dissipated energy [Fig. 2(b)]. The larger the interpenetration, also referred to as *overlapping* in the sequel, the lower the transferred forces along the damaged zone.

Cohesive Crack Model for the Description of Concrete Fracturing

Linear elastic fracture mechanics has been proven to be a useful tool for solving fracture problems, provided that a crack-like notch or flaw exists in the body and that the nonlinear zone ahead of the crack tip is negligible. These conditions are not always fulfilled and, both for metallic and cementitious materials, the size of the process zone due to plasticity or microcracking can be not negligible with respect to the dimensions of the structural element. In such conditions, the localized damaged material can be modeled as a pair of restrained fracture surfaces. This idea has been extensively applied to materials that are commonly classified as quasi-brittle, such as concrete, rocks, glass, polymers, etc. In particular, the most suitable model for concrete was first proposed by Hillerborg et al. (1976) with the name of *fictitious crack model*. Afterward, Carpinteri (1985, 1989), proposed an updated algorithm referred to as *cohesive crack model* for the study of ductile-brittle transition and snap-back instability in concrete elements in bending.

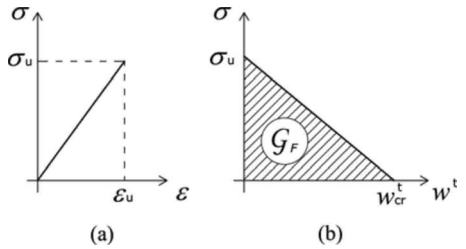

Fig. 3. Cohesive crack model for concrete in tension: (a) linear–elastic $\sigma-\varepsilon$ law and postpeak; (b) softening $\sigma-w$ relationship

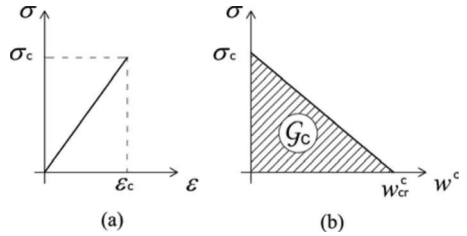

Fig. 4. Overlapping crack model for concrete in compression: (a) linear–elastic $\sigma-\varepsilon$ law; (b) postpeak softening $\sigma-w$ relationship

The main hypotheses of the model can be summarized as follows:

1. The constitutive law used for the nondamaged zone is the $\sigma-\varepsilon$ linear–elastic relationship shown in Fig. 3(a);
2. The process zone develops when the maximum stress reaches the ultimate tensile strength;
3. The process zone is perpendicular to the main tensile stress; and
4. In the process zone, the damaged material is still able to transfer a tensile stress across the crack surfaces. The cohesive stresses are considered to be decreasing functions of the crack opening w^t [see Fig. 3(b)]

$$\sigma = \sigma_u\left(1 - \frac{w^t}{w^t_{\rm cr}}\right) \tag{1}$$

where w^t=crack opening; $w^t_{\rm cr}$=its critical value corresponding to the condition $\sigma=0$; and σ_u=ultimate tensile strength of concrete.

The shaded area under the stress versus displacement curve in Fig. 3(b) represents the fracture energy, G_F.

Overlapping Crack Model for the Description of Concrete Crushing

The most frequently adopted constitutive laws for concrete in compression describe the material behavior in terms of stress and strain. This approach implies that the energy is dissipated over a volume, whereas experimental results reveal that the energy is mainly dissipated over a surface. Hillerborg (1990) first proposed to model the crushing phenomenon as a strain localization over a length proportional to the depth of the compression zone. However, the evaluation of this characteristic length is rather complicated by the fact that the depth of the compressed zone is not constant, but varies during the flexural loading process. As a result, it is difficult to formulate a material constitutive law fully describing the mechanical response of concrete in compression.

In the present formulation, we introduce a stress–displacement relationship between compression stress and interpenetration, in close analogy with the cohesive model. The main hypotheses are the following:

1. The constitutive law used for the undamaged material is a linear-elastic stress-strain relationship, see Fig. 4(a);
2. The crushing zone develops when the maximum compression stress achieves the concrete compression strength;
3. The process zone is perpendicular to the main compression stress; and
4. The damaged material in the process zone is assumed to be able to transfer a compression stress between the overlapping surfaces. Concerning the crushing stresses, they are assumed to be a decreasing function of the interpenetration w^c [see Fig. 4(b)]

$$\sigma = \sigma_c\left(1 - \frac{w^c}{w^c_{\rm cr}}\right) \tag{2}$$

where w^c=interpenetration; $w^c_{\rm cr}$=its critical value corresponding to the condition $\sigma=0$; and σ_c=ultimate compression strength. This zone is then represented by a fictitious overlapping, that is mathematically analogous to the fictitious crack in tension, as shown in Fig. 5.

It is important to note that, from a mathematical point of view, the overlapping displacement is a global quantity, and therefore it permits us to characterize the structural behavior without the need of modeling into the details the actual failure mode of the specimen, which may vary from pure crushing to diagonal shear or to splitting failures, depending on its size-scale and/or slenderness. The proposed model, based on a fictitious interpenetration, permits to obtain a true material constitutive law, independent of the structural size [see the experimental confirmation by van Vliet and van Mier (1996) and by Jansen and Shah (1997)]. Therefore, with respect previous approaches, the proposed methodology applied to RC beams in bending has the advantage to avoid the elaborate description of the kinematics of the failure mode (see, e.g., the detailed description of the triangular-shaped failure surface expelled during crushing by Fantilli et al. 2007).

In analogy with the *cohesive crack model*, we can define the area under the stress–displacement curve as the crushing energy, G_C. Dahl and Brincker (1989) carried out a series of uniaxial compression tests with the aim of measuring the dissipated energy per unit cross-sectional area. They obtained values of about 50 N/mm and claimed that this dissipated energy becomes independent of the specimen size if the specimen is large enough. A more sophisticated stress–displacement law considering the phenomenon of compacting was recently proposed by Suzuki et al. (2006). In this case, the crushing energy is computed according to the following empirical equation, which considers the confined concrete compression strength by means of the stirrups yield strength and the stirrups volumetric content:

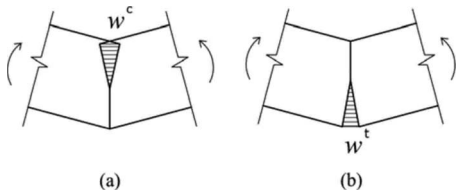

Fig. 5. (a) Compression crushing with overlapping; (b) tensile fracture with cohesive zone

Table 1. Comparison between Crushing Energy and Fracture Energy for Different Concrete Compression Strengths

σ_c (N/mm^2)	$\mathcal{G}_{C,0}$ (N/mm)	$\mathcal{G}_F$ (N/mm)
30	30	0.065
50	40	0.090
70	51	0.117
90	58	0.140

$$\frac{G_C}{\sigma_c} = \frac{G_{C,0}}{\sigma_c} + 10{,}000\frac{k_a^2 p_e}{\sigma_c^2} \tag{3a}$$

where σ_c=average concrete compression strength; k_a=parameter depending on the stirrups strength and volumetric percentage; and p_e=effective lateral pressure. The crushing energy for unconfined concrete, $G_{C,0}$, can be calculated using the following expression:

$$G_{C,0} = 80 - 50k_b \tag{3b}$$

where the parameter k_b depends on the concrete compression strength.

A comparison between crushing energy and fracture energy for different compression strengths is proposed in Table 1. The crushing energy is calculated according to Eq. (3*b*) for concrete without stirrups, whereas the fracture energy is calculated according to the CEB-FIP Model Code 90 in the case of a maximum aggregate dimension of 16 mm. It is worth noting that G_C is between 2 and 3 orders of magnitude higher than G_F. Finally, we remark that the critical values for crushing interpenetration and crack opening are, respectively, equal to $w_{cr}^c \approx 1$ mm [see also the experimental results in Jansen and Shah 1997] and $w_{cr}^t \approx 0.1$ mm. The effect of the lateral reinforcement and its spacing can be indirectly taken into account in the model as a modification of the crushing energy.

Steel–Concrete Interaction

In order to model the steel contribution to the load carrying capacity of the beam, it is necessary to introduce a suitable bond–slip law for the characterization of steel–concrete interaction. Typical bond–slip relationships are defined in terms of a tangential stress along the steel–concrete interface as a function of the relative tangential displacement between the two materials (see Jenq and Shah 1989; CE-FIP 1990; Carpinteri 1999). The integration of the differential slip over the transfer length, l_{tr}, is equal to one-half of the opening crack at the reinforcement level. On the other hand, the integration of the bond stresses gives the reinforcement reaction. In order to simplify the calculation, the stress–displacement law is herein assumed to be linear until the yield stress (or until the critical crack opening for steel, w_y) is

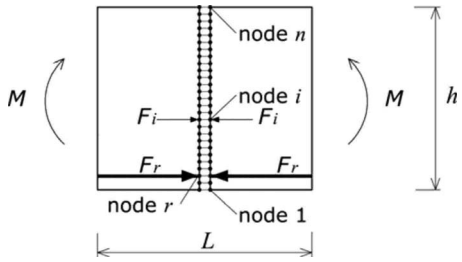

Fig. 6. Finite-element nodes along the midspan cross section

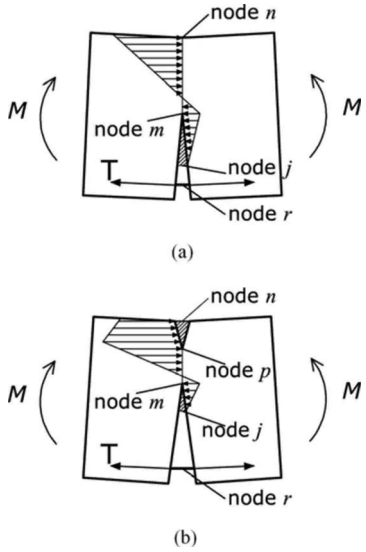

Fig. 7. Force distribution with: (a) cohesive crack in tension and linear elastic behavior in compression; (b) cohesive crack in tension and crushing in compression

achieved. After that, the reinforcement reaction is considered to be constant, until the crack-opening displacement at the reinforcement level reaches a limit value corresponding to steel rupture.

Numerical Algorithm

A discrete form of the elastic equations governing the mechanical response of the two half-beams is herein introduced in order to develop a suitable algorithm for the analysis of all the intermediate situations, where both fracturing and crushing phenomena take place. The midspan cross section of the beam can be subdivided into finite elements by n nodes. (Fig. 6). In this scheme, cohesive and overlapping stresses are replaced by equivalent nodal forces by integrating the corresponding tractions over the element size. Such nodal forces depend on the nodal opening or closing displacements according to the cohesive or overlapping softening laws shown, respectively, in Figs. 3(b) and 4(b).

The horizontal forces, F, acting along the midspan cross section can be computed as follows:

$$\{F\} = [K_w]\{w\} + \{K_M\}M \tag{4}$$

where $\{F\}$=vector of nodal forces; $[K_w]$=matrix of the coefficients of influence for the nodal displacements, $\{w\}$=vector of nodal displacements; $\{K_M\}$=vector of the coefficients of influence for the applied moment; and M=applied moment. The coefficients of influence $[K_w]$ have the physical dimension of a stiffness and are computed a priori with a finite-element analysis by applying a unitary displacement to each of the nodes shown in Fig. 6. The reinforcement contribution is also included in the nodal force corresponding to the rth node.

In the generic situation shown in Fig. 7(a), the following equations can be considered:

$$F_i = 0 \quad \text{for } i = 1,2,\ldots,(j-1); \quad i \neq r \tag{5a}$$

$$F_i = F_u\left(1 - \frac{w_i^t}{w_{cr}^t}\right) \quad \text{for } i = j,\ldots,(m-1) \tag{5b}$$

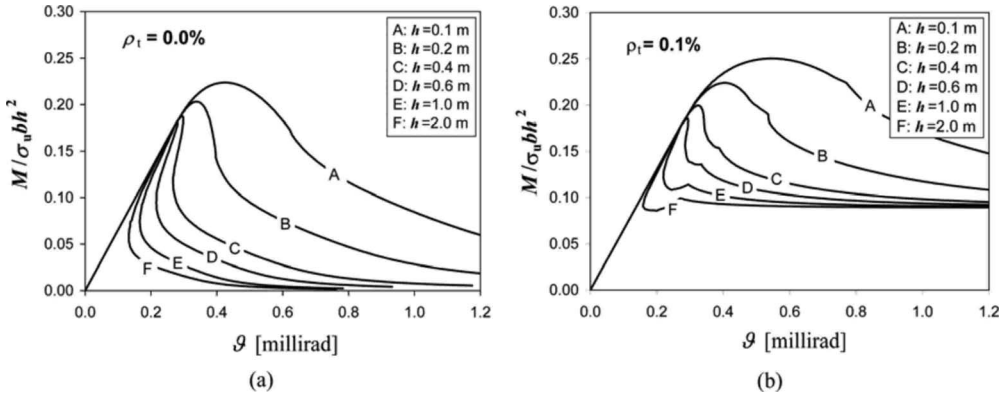

Fig. 8. Nondimensional moment versus rotation diagrams in case of (a) ρ_t=0.0%; (b) ρ_t=0.1%

$$w_i = 0 \quad \text{for } i = m, \ldots, n \tag{5c}$$

Eqs. (4) and (5) constitute a linear algebraic system of $(2n)$ equations and $(2n+1)$ unknowns, i.e., the elements of the vectors $\{w\}$ and $\{F\}$ and the applied moment, M. The additional equation required to solve the problem is obtained by setting the value of the force at the fictitious crack tip, say m, equal to the ultimate tensile force. The driving parameter of the process is the position of the fictitious crack tip, defined by the position of the node m in Fig. 7(a), which is increased by one nodal position at each step of the algorithm. Hence, the position of the real crack tip, j, turns out to be a function of the crack opening.

When crushing takes place [see Fig. 7(b)], the equation set (5) is replaced by

$$F_i = 0 \quad \text{for } i = 1,2, \ldots, (j-1); \quad i \neq r \tag{6a}$$

$$F_i = F_u\left(1 - \frac{w_i^t}{w_{\text{cr}}^t}\right) \quad \text{for } i = j, \ldots, (m-1) \tag{6b}$$

$$w_i = 0 \quad \text{for } i = m, \ldots, p \tag{6c}$$

$$F_i = F_c\left(1 - \frac{w_i^c}{w_{\text{cr}}^c}\right) \quad \text{for } i = (p+1), \ldots, n \tag{6d}$$

where the superscripts t and c stand for tension or compression, respectively.

Again, Eqs. (4) and (6) constitute a linear algebraic system of $(2n)$ equations and $(2n+1)$ unknowns. In this case, there are two possible additional equations: we can set either the force in the fictitious crack tip, m, equal to the ultimate tensile force, or the force in the fictitious crushing tip, p, equal to the ultimate compression force. In the numerical scheme, we choose the situation that is the closest to one of these two critical conditions. The driving parameter of the process is the tip that in the considered step has reached the limit resistance. Only this tip is moved when passing to the next step.

The two fictitious tips advance until they converge to the same node. So forth, in order to describe the descending branch of the moment–rotation diagram, the two tips can move together toward the soffit of the beam. As a consequence, the crack in tension closes and the overlapping zone is allowed to extend toward the soffit. This situation is quite commonly observed in overreinforced beams, where steel yielding does not take place.

Finally, at each step of the algorithm it is possible to calculate the beam rotation, ϑ, as follows:

$$\vartheta = \{D_w\}^T\{w\} + D_M M \tag{7}$$

where $\{D_w\}$=vector of the coefficients of influence for the nodal displacements and D_M=coefficient of influence for the applied moment. The physical dimensions of the coefficients D_w^i and D_M are, respectively $[\text{L}]^{-1}$ and $[\text{F}^{-1}\,\text{L}]^{-1}$.

Parametric Study

In this section, the results of the numerical simulations are shown. They are carried out to investigate the influence of two fundamental parameters on the global mechanical behavior of RC beams in bending, namely the beam size and the tensile steel percentage. In the numerical scheme, the midspan cross section is discretized into 160 elements and the coefficients of influence entering Eq. (4) are preliminarily determined using the finite-element method. The length-to-overall depth ratio, λ, and the thickness, b, are kept constant in the following examples and equal, respectively, to 1 and 200 mm. The following mechanical parameters are assumed for concrete: σ_c=40 MPa, G_c=30 N/mm, σ_u=4 MPa, G_F=0.08 N/mm. The tensile yield strength of steel, σ_y, is set equal to 400 MPa. In the parametric study, the reinforcement ratio, ρ_t, has been varied from 0 to 3%, simulating all the intermediate situations from plain concrete beams to overreinforced beams, whereas the beam depth, h, has been varied from 0.1 to 2 m. The ratio between effective depth, d, and overall depth, h, is kept constant and equal to 0.9.

In the limit case characterized by ρ_t=0%, the curves obtained using the *cohesive crack model* by Carpinteri et al. (1986) are perfectly recovered by the present model, as shown in Fig. 8(a). The normalization of the vertical axis is chosen in order to highlight the ductile-to-brittle transition by varying the structural size. The beams with a depth ranging from 0.1 to 0.4 m exhibit a softening behavior. By increasing again the beam depth, i.e., from 0.4 to 2.0 m, a snap-back instability is observed. Similar results are observed in the case of ρ_t=0.1% as shown in Fig. 8(b). In this case, however, a horizontal asymptote different from zero exists, due to the effect of the steel contribution.

In general, in the case of low steel percentages, crushing does not take place and a single nondimensional parameter, like the brittleness number N_P, as defined by Carpinteri (1981, 1984), can be used to describe the transition from ductile to brittle behaviors:

$$N_P = \rho_t \frac{\sigma_y h^{0.5}}{\sqrt{G_F E_c}} \tag{8}$$

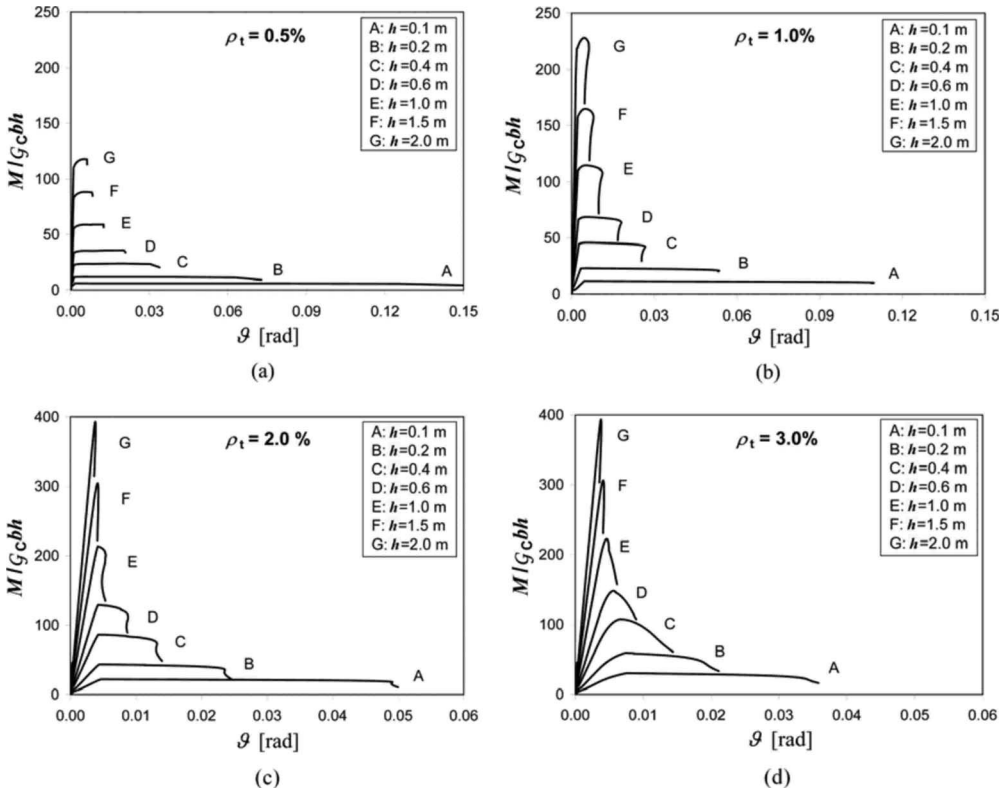

Fig. 9. Nondimensional moment versus rotation diagrams in case of: (a) ρ_t=0.5%; (b) ρ_t=1.0%; (c) ρ_t=2.0%; and (d) ρ_t=3.0%

The diagrams shown in Fig. 9(a) are related to a reinforcement ratio equal to 0.5%. A plateau is observed in the nondimensional bending moment versus rotation diagram when steel yielding occurs. The normalization of the vertical axis is different from that assumed in Fig. 8 only for graphical reasons. These curves put into evidence that the beam rotation at failure is progressively diminished by increasing the beam depth, with the appearance of steeper and steeper softening branches. It is worth noting that design codes consider the dependence of the ultimate rotation on the steel percentage and on the beam slenderness, whereas the structural dimension is not taken into account. In the case of ρ_t=0.5%, the reinforcement reaches the ultimate deformation for any beam depths, whereas concrete crushing is not particularly important.

However, by increasing the reinforcement ratio, as for ρ_t=1.0, 2.0, and 3.0% [see Figs. 9(b–d)], the steel deformation at failure progressively decreases and concrete crushing becomes more and more predominant, leading to severe brittle behaviors after the achievement of the peak load. As a result, the ductility, which can be conventionally measured through the extension of the plateau after the peak load, turns out to be a decreasing function of the steel percentage. The smallest beam with h=0.1 m maintains a discrete rotational capacity also with very high steel percentage [see Fig. 9(d)]. In this case, as steel yielding does not take place, the only contribution to ductility is due to concrete crushing.

Comparison with Experimental Results

The testing program herein considered was carried out by Bosco and Debernardi in the Materials and Structures Laboratory of the Department of Structural Engineering and Geotechnics of the Politecnico di Torino Italy on 22 simply supported RC beams (Bosco and Debernardi 1992). Three different structural scales of the beams were considered, with cross-section depths of 200, 400, and 600 mm and constant slenderness l/h=10. The percentage of tensile reinforcement was varied between 0.13 and 1.70%. The characteristics of stirrups and compression reinforcement, ρ_c, are given in Table 2.

The width-to-depth ratio of the beam cross section, b/h=0.5, the effective depth-to-total depth ratio, d/h=0.9 and the diameter of the tension bars, ϕ=12 mm, were kept constant. The instrumentation included two linear potentiometers (Devices 7 and 12 in Fig. 10) for measuring the deformations at the top and bottom sides of the beam. The length of each extensimeter was equal to the beam depth. By means of such an instrumentation, the

Table 2. Mechanical and Geometrical Parameters of the Beams Tested by Bosco and Debernardi (1992)

Beam	h (mm)	b (mm)	L (mm)	ρ_t (%)	ρ_c (%)	Stirrups	$\mathcal{G}_{C,0}$ (N/mm)
T1	200	100	2,000	0.57	0.25	ϕ 6/15	53
T2				1.13	0.50	ϕ 6/15	
T3				1.71	0.50	ϕ 6/15	
T4	400	200	4,000	0.28	0.20	ϕ 6/20	30
T5				0.57	0.20	ϕ 6/20	
T6				1.13	0.20	ϕ 6/20	
T7				1.71	0.30	ϕ 6/20	
T8	600	300	6,000	0.13	0.12	ϕ 6/15	48
T9				0.25	0.12	ϕ 6/15	
T10				0.57	0.12	ϕ 6/15	
T11				1.13	0.12	ϕ 6/15	

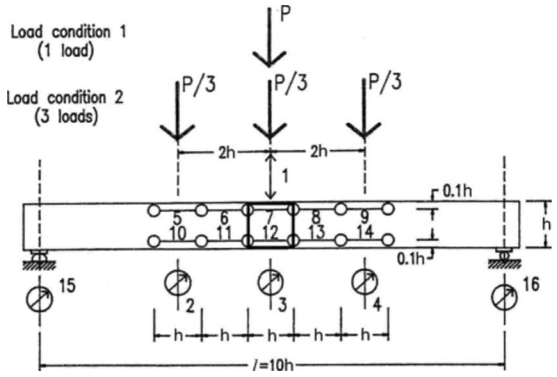

Fig. 10. Testing scheme and loading conditions in Bosco and Debernardi (1992)

rotation of the midspan region, characterized by a length equal to the depth, can be directly evaluated as the difference between the longitudinal displacements at the soffit and at the extrados, divided by the total beam depth. The reinforcing bars have the following mechanical parameters: yield strength, f_{ym} =587 N/mm^2, failure stress, f_{tm}=672 N/mm^2 and strain at failure load, ε_{su}=7.0%. The mean compression strength of concrete, measured at 60 days on ten 16 cm side cubes, was equal to 30.9 N/mm^2 with a standard deviation of 1.10 N/mm^2. The concrete tensile strength was measured on six samples through splitting tensile tests and its average value was equal to 2.97 N/mm^2 with standard deviation of 0.5 N/mm^2. The outcome of the testing program is represented by the bending moment versus rotation diagram of the central portion of the beams.

The numerical simulations have been carried out by modelling the central beam region characterized by a span-to-depth ratio equal to unity, in order to obtain a consistent comparison with experimental measures (see Fig. 10). The values of the crushing energy, determined according to Eq. (3*a*), taking into account the stirrups confinement, are reported in Table 2.

The numerical and experimental moment–rotation curves are compared in Fig. 11 for different beam depths and different steel percentages. These diagrams put into evidence that the maximum rotation is a decreasing function of the tensile reinforcement ratio and of the beam depth. In the case of low steel percentages, the mechanical behavior is characterized by reinforcement yielding and the mechanical response is almost plastic. By increasing the amount of reinforcement, the contribution of concrete crushing becomes more and more evident with the appearance of a softening branch at the end of the plastic plateau. This is an important feature of the proposed model, which also permits us to follow unstable softening branches with positive slopes (snap-back) by controlling the loading process through the length of the tensile crack and the extension of the fictitious crushing zone, rather than by the external load. Hence, this numerical method permits to overcome some drawbacks of the classical approaches based on elastoplasticity that are traditionally used to model the constitu-

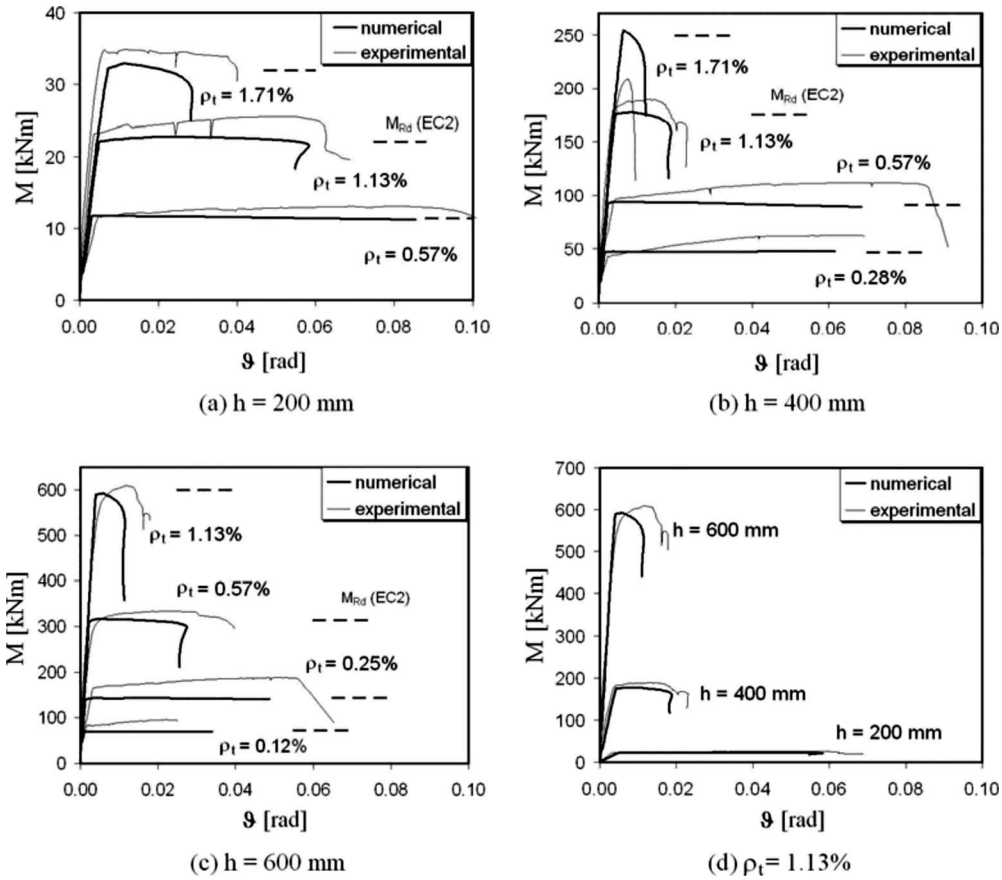

Fig. 11. Numerical and experimental moment versus rotation diagrams for the beams tested by Bosco and Debernardi (1992). The experimental curves have been obtained from the original moment-curvature data in Bosco and Debernardi (1992) by integrating the curvatures along the beam portion.

tive behavior of concrete in compression (see Barbosa and Ribeiro 1998). To model this nonlinear process, in fact, the Drucker–Prager yield criterion or improved versions are adopted to model the local behavior of the material and iterative algorithms have to be invoked. However, the parameters defining the yield surface have to be updated during the loading process in order to capture the softening response of the material, making extremely difficult the analysis of unstable postpeak responses [see the material identification procedure proposed by Cela (2002) for uniaxial compression tests].

The numerically predicted maximum resistant moments are very often lower than the experimental ones, as we can see in Figs. 11(a–c). This is due to the fact that the hardening behavior of steel before yielding is not taken into account in the numerical model. On the other hand, a good agreement is obtained with the ultimate resistant moment calculated in accordance with the Eurocode 2 prescriptions (parabolic–perfectly plastic relationship for concrete in compression and elasto plastic relationship for steel), whose values are reported with dashed lines in Figs. 11(a–c). The size-scale effect is put into evidence in Fig. 11(d) by keeping constant the steel percentage equal to 1.13% and varying the beam depth from 200 to 600 mm. A general good agreement is obtained between numerical and experimental results for all the tested beams, with no significant differences between the two considered loading cases shown in Fig. 10.

Discussion and Conclusions

In the present paper, a general numerical algorithm has been proposed for the analysis of the mechanical behavior of RC elements in bending, ranging from pure concrete to overreinforced concrete beams. To this aim, all the main nonlinear contributions are taken into account for an accurate evaluation of the moment–rotation diagram. This model can be profitably applied to model the beam regions subjected to a high gradient in the bending moment diagram, where a plastic hinge formation takes place, as, e.g., the middle portion of a three-point bending beam or the regions close to the intermediate supports. The following main conclusions can be drawn from the results of the parametric analysis.

1. The introduced constitutive law for concrete in compression through the *overlapping crack model* permits us to describe the descending branch of the moment–rotation diagram for over-reinforced beams.
2. Referring to Figs. 8 and 9, it is possible to state that, independently of the reinforcement ratio, the behavior becomes more and more brittle by increasing the beam depth. This is very well evidenced by a progressive reduction of the beam rotation at failure. Such size-scale effects are not considered in the actual design codes. For instance, by applying the model code, the position of the neutral axis at the ultimate condition, and consequently the plastic rotation determined as a function of the neutral axis position, are independent of the beam depth. They depend only on the steel percentage. With the proposed algorithm, the position of the neutral axis is found to be dependent on the beam depth.
3. By varying the steel percentage, a double transition is evidenced: a brittle behavior in the case of very low steel percentages, a ductile behavior in the case of medium steel percentages, and again a brittle response for high steel percentages, this time due to concrete crushing.
4. Referring to Fig. 11, it is possible to state that the proposed algorithm catches the experimental results by varying both the structural dimension and the steel percentage.

Future developments of the present model will regard the analysis of the plastic rotation, as defined by Corley (1966), Macchi (1969), and Eligehausen and Langer (1987), as a measure of the ductility of RC elements in bending. The effect of the statistical variability of the mechanical parameters on the structural response will also be investigated. In this stage, further numerical/experimental comparison will be carried out in order to highlight the possible limitations of the present approach.

Acknowledgments

The financial support provided by the European Union to the Leonardo da Vinci Project "Innovative Learning and Training on Fracture" (ILTOF) is gratefully acknowledged.

Notation

The followings symbols are used in this paper:

b = thickness of the beam;
D_M = coefficient of influence for the applied moment;
$\{D_w\}^T$ = vector of the coefficients of influence for the nodal displacements;
d = effective depth of the beam;
$\{F\}$ = vector of nodal forces;
F_c = ultimate compression force;
F_u = ultimate tensile force;
G_C = crushing energy of confined concrete;
$G_{C,0}$ = crushing energy of unconfined concrete;
G_F = fracture energy;
h = overall depth of the beam;
$\{K_M\}$ = vector of the coefficients of influence for the applied moment;
$[K_w]$ = matrix of the coefficients of influence for the nodal displacements;
L = specimen span;
M = applied bending moment;
N_P = brittleness number for underreinforced concrete;
$\{w\}$ = vector of nodal displacements;
w^c = overlapping displacement;
w^c_{cr} = critical overlapping displacement;
w^t = crack-opening displacement;
w^t_{cr} = critical crack-opening displacement;
ϑ = RC element rotation;
λ = L/h, specimen slenderness;
ρ_c = A'_s/bh, compression steel percentage;
ρ_t = A_s/bh, tensile steel percentage;
σ = stress in concrete;
σ_c = compression strength of concrete;
σ_u = tensile strength of concrete; and
σ_y = tensile yield strength of steel.

References

Barbosa, A. F., and Ribeiro, G. O. (1998). "Analysis of reinforced concrete structures using ANSYS nonlinear concrete model." *Computational Mechanics: New trends and applications*, S. Idelsohn, E. Onate, and E. Dvorkin, eds., CIMNE, Barcelona, Spain, 1–7.

Bazant, Z. P., and Kim, J. K. (1984). "Size effect in shear failure of longitudinally reinforced beams." *ACI J.*, 81(5), 456–468.
Bigaj, A. J., and Walraven, J. C. (1993). "Size effect on rotational capacity of plastic hinges in reinforced concrete beams." *CEB Bulletin d'Information No. 218*, Lausanne, Switzerland, 7-23.
Bosco, C., and Carpinteri, A. (1992). "Softening and snap-through behavior of reinforced elements." *J. Eng. Mech.*, 118(8), 1564–1577.
Bosco, C., Carpinteri, A., and Debernardi, P. G. (1990). "Minimum reinforcement in high strength concrete." *J. Struct. Eng.*, 116(2), 427–437.
Bosco, C., and Debernardi, P. G. (1992). "Experimental investigation on the ultimate rotational capacity of RC beams." *Rep. No. 36*, Atti del Dipartimento, Politecnico di Torino, Ingegneria Strutturale.
Carpinteri, A. (1981). "A fracture mechanics model for reinforced concrete collapse." *Proc., IABSE Colloquium*, Delft University Press, Delft, The Netherlands, 17–30.
Carpinteri, A. (1984). "Stability of fracturing process in RC beam." *J. Struct. Eng.*, 110(3), 544–558.
Carpinteri, A. (1985). "Interpretation of the Griffith instability as a bifurcation of the global equilibrium." *Proc., NATO Advanced Research Workshop on Application of Fracture Mechanics to Cementitious Composites*, S. P. Shah, ed., Martinus Nijhoff Publishers, Dordrecht, The Netherlands, 287–316.
Carpinteri, A. (1989). "Size effects on strength, toughness, and ductility." *J. Eng. Mech.*, 115(7), 1375–1392.
Carpinteri, A., ed. (1999). *Minimum reinforcement in concrete members*, Elsevier Science Ltd., Oxford, U.K., VIII +203.
Carpinteri, A., Di Tommaso, A., and Fanelli, M. (1986). "Influence of material parameters and geometry on cohesive crack propagation." *Fracture toughness and fracture energy of concrete*, F. H. Wittmann, ed., Elsevier, Amsterdam, The Netherlands, 117–135.
Carpinteri, A., Ferro, G., and Ventura, G. (2005). "Scale-independent constitutive law for concrete in compression." *Proc., 11th Int. Conf. on Fracture (ICF)* (CD-ROM), A. Carpinteri, ed., Trading, Torino, Italy, Paper No. 5556.
Carpinteri, A., Ventura, G., and Carmona, J. R. (2007). "Flexural to shear and crushing failure transitions in RC beams by the bridged crack model." *Proc., 6th Int. FraMCoS Conf.*, Vol. 2, A. Carpinteri, P. Gambarova, G. Ferro, and G. Plizzari, eds., Taylor & Francis, Catania, Italy, 677–684.
Cela, J. J. L. (2002). "Material identification procedure for elastoplastic Drucker-Prager model." *J. Eng. Mech.*, 128(5), 586–591.
Comité Euro–International du Béton. (1993). *CEB-FIP Model Code 1990*, Thomas Telford, Ltd., Lausanne, Switzerland.
Corley, W. G. (1966). "Rotational capacity of reinforced concrete beams." *J. Struct. Div.*, 92(ST5), 121–146.
Dahl, H., and Brincker, R. (1989) "Fracture energy of high-strength concrete in compression." *Proc., Int. Conf. on Recent Developments in the Fracture of Concrete and Rock*, S. P. Shah, S. E. Swartz, and B. Barr, eds., Elsevier Applied Science, Cardiff, U.K., 523–536.
Eligehausen, R., and Langer, P. (1987). "Rotation capacity of plastic hinges and allowable degree of moment redistribution." *CEB Bulletin d'Information No. 175*, Lausanne, Switzerland, 93-102.
EN. (1992). "Eurocode 2: Design of concrete structures—Part 1-1: General rules and rules for buildings." *EN 1992-1-1, 5.6.3*, *Rotation Capacity*, Brussels.
Fantilli, A. P., Iori, I., and Vallini, P. (2007). "Size effect of compressed concrete in four point bending RC beams." *Eng. Fract. Mech.*, 74(1–2), 97–108.
Gustafsson, P. J., and Hillerborg, A. (1988). "Sensitivity in shear strength of longitudinally reinforced concrete beams energy of concrete." *ACI Struct. J.*, 85(3), 286–294.
Hillerborg, A. (1990). "Fracture mechanics concepts applied to moment capacity and rotational capacity of reinforced concrete beams." *Eng. Fract. Mech.*, 35(1/2/3), 233–240.
Hillerborg, A., Modeer, M., and Petersson, P. E. (1976). "Analysis of crack formation and crack growth in concrete by means of fracture mechanics and finite elements." *Cem. Concr. Res.*, 6(6), 773–782.
Jansen, C. D., and Shah, S. P. (1997). "Effect of length on compressive strain softening of concrete." *J. Eng. Mech.*, 123(1), 25–35.
Jenq, Y. S., and Shah, S. P. (1989). "Shear resistance of reinforced concrete beams—a fracture mechanics approach." *Fracture mechanics: Application to concrete*, V. C. Li and Z. P. Bazant, eds., American Concrete Institute, Detroit, 327–358.
Macchi, G. (1969). "Limit-states design of statically indeterminate structures composed of linear members." *Costruzioni in Cemento Armato, Studi e Rendinconti*, 6, 151–190.
Suzuki, M., Akiyama, M., Matsuzaki, H., and Dang, T. H. (2006). "Concentric loading test of RC columns with normal- and high-strength materials and averaged stress-strain model for confined concrete considering compressive fracture energy." *Proc., 2nd fib Int. Conf.* (CD-ROM), Doppiavoce, Napoli, Italy, ID 3–13.
van Vliet, M., and van Mier, J. (1996). "Experimental investigation of concrete fracture under uniaxial compression." *Mech. Cohesive-Fricț. Mater.*, 1(1), 115–127.